Journal of
Materials Chemistry C

PAPER

View Article Online
View Journal

Cite this: DOI: 10.1039/c7tc00299h

Lead monoxide: a two-dimensional ferromagnetic semiconductor induced by hole-doping

Yao Wang,[a] Qingyun Zhang,[b] Qian Shen,*[a] Yingchun Cheng,*[a] Udo Schwingenschlögl[b] and Wei Huang[a]

Received 18th January 2017,
Accepted 11th April 2017

DOI: 10.1039/c7tc00299h

rsc.li/materials-c

We employ first-principles calculations to demonstrate ferromagnetic ground states for single- and multi-layer lead monoxide (PbO) under hole-doping, originating from a van Hove singularity at the valence band edge. Both the sample thickness and applied strain are found to have huge effects on the electronic and magnetic properties. Multi-layer PbO is an indirect band gap semiconductor, while a direct band gap is realized in the single-layer limit. In hole-doped single-layer PbO, biaxial tensile strain can enhance the stability of the ferromagnetic state.

Introduction

Nowadays extensive research efforts focus on the development of novel two-dimensional (2D) materials, including semiconducting metal monochalcogenides MX (M = Ge, Sn; X = S, Se, Te)[1–8] and transition metal dichalcogenides TX_2 (T = Mo, W; X = S, Se, Te),[9–16] with properties superior to the corresponding bulk compounds. Theoretical studies have shown that single-layer MX and TX_2 exhibit wide band gaps due to quantum confinement, giant spin splitting due to inversion symmetry breaking, and strong spin–orbit coupling.[17–20] An ultimate goal of 2D semiconductor research is control of the spin degree of freedom to design spintronics devices that utilize both the charge and spin of carriers.[21–23] Magnetism in 2D materials can be achieved by doping of magnetic atoms,[24,25] defects,[26–28] and strain engineering.[29,30] Recently, single-layer GaSe and GaS[31,32] have been reported to develop ferromagnetism under hole doping.

Metal oxides, the largest class of compounds on earth, are widely known for exotic magnetism and superconductivity, for example,[33–36] but not for 2D semiconductors. Therefore, it is of great interest that Singh and Hennig[37] have demonstrated that single-layer lead monoxide (PbO) has a stable tetragonal litharge structure with a direct band gap. Because a systematic study of PbO is missing, we investigate in the present work the influence of the thickness as well as the effects of strain and hole doping on the electronic structure by means of *ab initio* calculations.

Methods

Ab initio calculations are performed using density functional theory in the generalized gradient approximation (GGA) with Perdew–Burke–Ernzerhof parametrization for the exchange–correlation functional with van der Waals correction,[38,39] as implemented in the Quantum-ESPRESSO package.[40] We employ ultrasoft pseudopotentials and a 40 Ry plane wave energy cutoff. The in-plane lattice constant is 4.01 Å, and a 20 Å thick vacuum slab is used to model single- and multi-layer PbO. The atomic coordinates are fully relaxed until all atomic forces have decreased below 0.01 eV $Å^{-1}$. For bulk and layered PbO, respectively, the Brillouin zone is sampled on a $6 \times 6 \times 4$ and $6 \times 6 \times 1$ k-point grid.

Results and discussion

Single-layer PbO has a tetragonal structure, as shown in Fig. 1(a and b), with Pb connected to four O atoms in a pyramidal form. Bulk and multi-layer PbO are constructed by stacking these layers, see Fig. 1(c). The 2D Brillouin zone is depicted in Fig. 1(d). According to Fig. 2, the band gap increases when the number of layers decreases. Bulk and multi-layer PbO exhibit

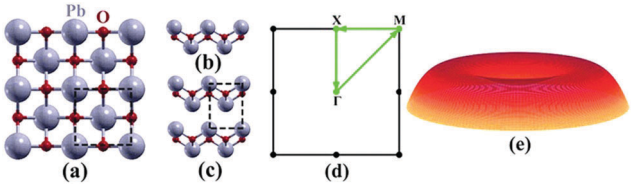

Fig. 1 (a) Top view of PbO. (b and c) Side views of single-layer and bulk PbO. (d) 2D Brillouin zone with high symmetry points. (e) Schematic representation of a Mexican-hat dispersion.

[a] Key Laboratory of Flexible Electronics (KLOFE) & Institute of Advanced Materials (IAM), Jiangsu National Synergetic Innovation Center for Advanced Materials (SICAM), Nanjing Tech University (NanjingTech), 30 South Puzhu Road, Nanjing 211816, China. E-mail: iamqshen@njtech.edu.cn, iamyccheng@njtech.edu.cn
[b] Physical Science and Engineering Division (PSE), King Abdullah University of Science and Technology (KAUST), Thuwal 23955-6900, Saudi Arabia

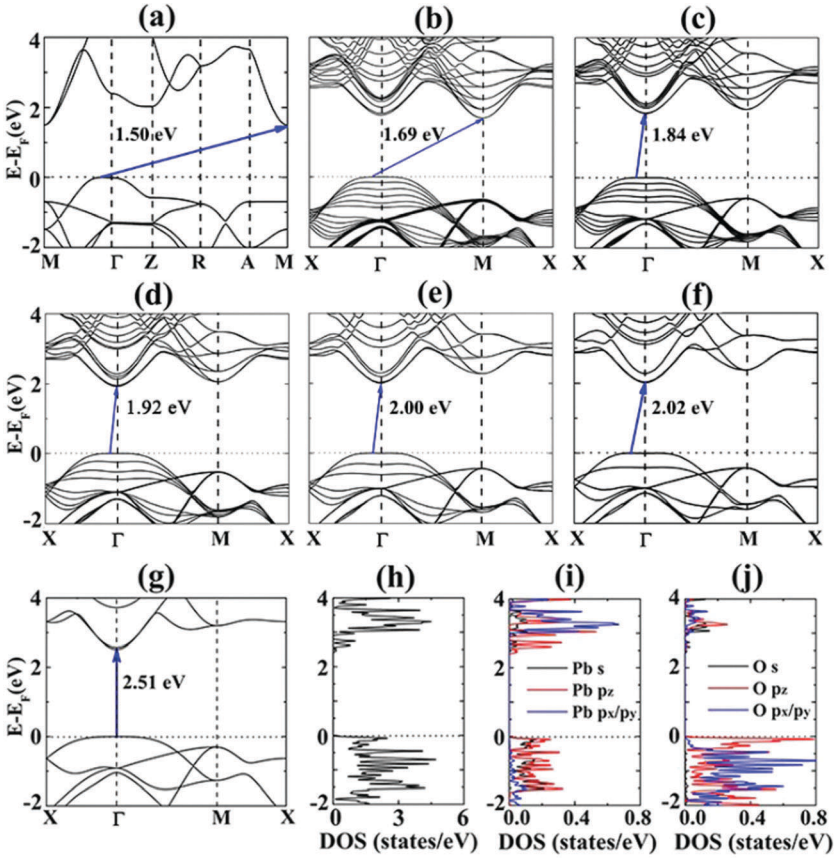

Fig. 2 Band structure of (a) bulk, (b) sextuple-, (c) quintuple-, (d) quadruple-, (e) triple-, (f) double-, and (g) single-layer PbO. The energy difference between the VBM and CBM is given. (h–j) DOS of single-layer PbO.

indirect band gaps, while transition to a direct band gap occurs in the single-layer limit. In the case of sextuple-layer PbO, Fig. 2(b) shows that the conduction band minimum (CBM) at the *M* point is only 0.09 eV below that at the Γ point. Reducing the number of layers shifts it to the Γ point. A Mexican-hat dispersion with a ring-like Fermi surface, see the schematic representation in Fig. 1(e), results in a van Hove singularity at the band edge.[25,31] This instability can induce ferromagnetism, superconductivity, and other phase transitions. Mexican-hat dispersions have been reported for many 2D materials,[41] including single-layer GaSe and GaS.[1,6] Fig. 2 demonstrates that the valence band maximum (VBM) stays near the Γ point for multi-layer PbO, reflecting a Mexican-hat dispersion. The energy difference between the VBM and highest occupied band at the Γ point is small, less than 8 meV, see Fig. 2(b–g). In the single-layer limit the VBM shifts to the Γ point, resulting in a direct band gap. Although the Mexican-hat dispersion disappears for single-layer PbO, the dispersion is rather flat at the VBM and the density of states (DOS) thus is high, as shown in Fig. 2(h). The DOS projected on the Pb and O atoms, see Fig. 2(i and j), indicates that the conduction band edge is largely due to the Pb p_z orbitals and the valence band edge due to the O p_z and Pb s, p_z orbitals.

Interestingly, we find that the band gap of single-layer PbO can be transformed from direct to indirect by biaxial tensile strain. Fig. 3(a–d) shows band structures for 3–6% strain. A transition occurs close to 3%, because the highest occupied band develops a dip at the Γ point (with the CBM remaining at the Γ point). This gives rise to a Mexican-hat dispersion similar to multi-layer PbO. The depth of the dip at the Γ point grows rapidly from 1 meV at 4% strain to 20 meV at 6% strain. Fig. 3(e–g) addresses the DOS under 6% strain to demonstrate that the orbital characters of the valence and conduction band edges have not changed. By comparing Fig. 2(h) and 3(e) we find that the DOS at the valence band edge (and thus the electronic instability) is enhanced by strain.

While unstrained single-layer PbO is nonmagnetic, the van Hove singularity at the valence band edge may induce ferromagnetism when the Fermi level is tuned by hole doping, which is confirmed by our calculations. The spin polarized total DOS of unstrained single-layer PbO with hole density 1.6×10^{14} cm^{-2} is depicted in Fig. 4(a) and that of single-layer PbO under 6% biaxial tensile strain with hole density 2.0×10^{14} cm^{-2} in Fig. 4(b). We observe in both cases a large exchange splitting. Hole doping alone maintains the orbital character of the valence band edge (O p_z and Pb s, p_z orbitals), whereas combination with strain enhances the weight of the O p_z and Pb s contributions, see Fig. 4(b–f), and the spatial localization of the states. It is worth noting that biaxial tensile strain strongly enhanced the exchange splitting (from 0.22 eV to 0.32 eV under 6% strain), see Fig. 4(a and b), and thus the stability of the ferromagnetic state.

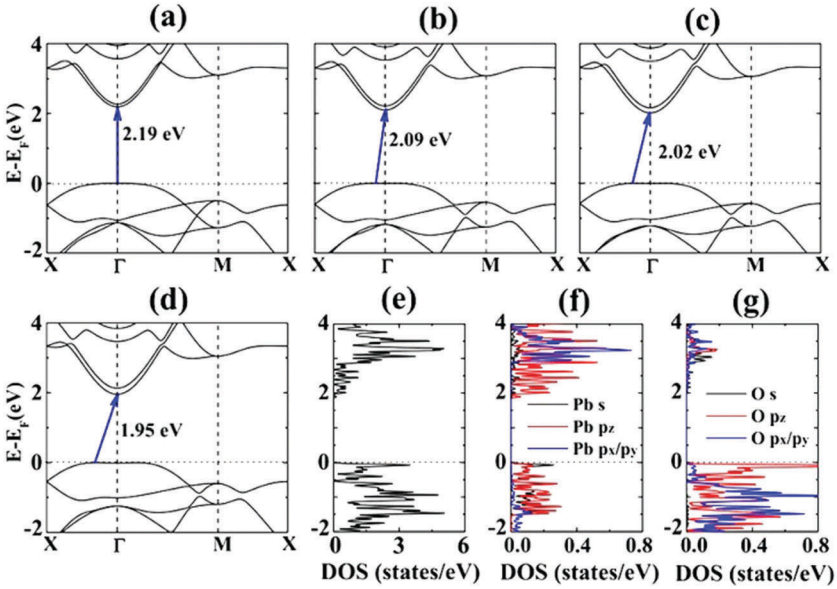

Fig. 3 Band structure of single-layer PbO under (a) 3%, (b) 4%, (c) 5%, and (d) 6% biaxial tensile strain. (e–g) DOS under 6% biaxial tensile strain.

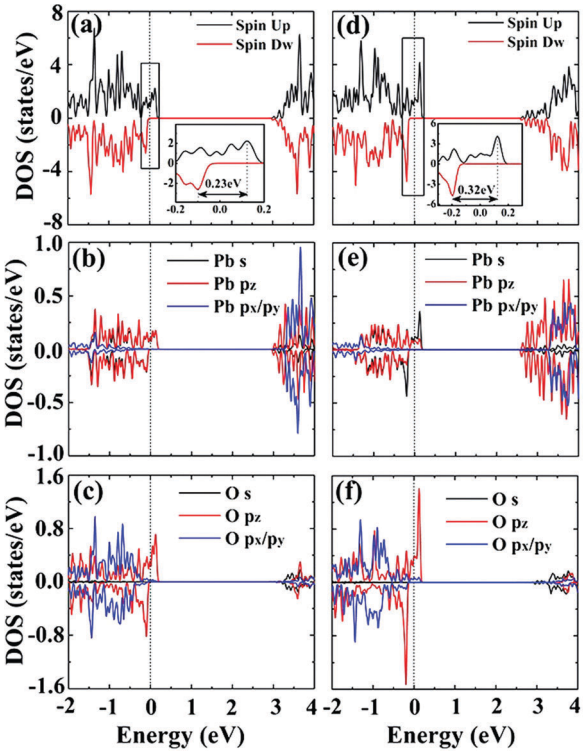

Fig. 4 Spin-resolved DOS of (a–c) unstrained single-layer PbO with hole density 1.6×10^{14} cm^{-2} and (d–f) single-layer PbO under 6% biaxial tensile strain with hole density 2.0×10^{14} cm^{-2}.

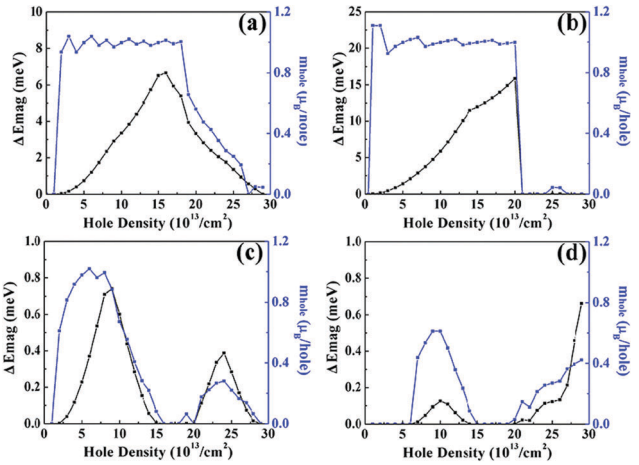

Fig. 5 Dependence of the polarization energy (black) and magnetic moment (blue) on the hole density: (a) unstrained single-layer PbO, (b) single-layer PbO under 6% biaxial tensile strain, (c) unstrained double-layer PbO, and (d) unstrained triple-layer PbO.

Calculating the total energy for nonmagnetic (E_{NM}), ferromagnetic (E_{FM}), and antiferromagnetic (E_{AFM}) phases, we check the stability of magnetization by determining the polar magnetic energy ΔE_{mag} as the energy difference $E_{NM} - E_{FM}$ for single-layer, and $E_{AFM} - E_{FM}$ for double- or triple-layer PbO.[35] A positive ΔE_{mag} reflects a preference for ferromagnetic ordering.

Fig. 5(a) shows that single-layer PbO turns ferromagnetic when the hole density reaches 0.2×10^{14} cm^{-2}, with a magnetic moment of $m = 0.93$ μ_B per hole. We find little changes up to a hole density of 1.9×10^{14} cm^{-2} and thereafter a slow reduction of m to zero. At a hole density of 2.7×10^{14} cm^{-2} the nonmagnetic state is restored. In the plateau region of m, ΔE_{mag} shows a distinct maximum of 6.7 meV at a hole density of 1.6×10^{14} cm^{-2} (highest stability of the ferromagnetic state). Under 6% biaxial tensile strain single-layer PbO turns ferromagnetic at a lower hole density of 0.1×10^{14} cm^{-2}, with $m = 1.1$ μ_B per hole, as shown in Fig. 5(b). We observe again a plateau region with $m \sim 1$ μ_B per hole, reaching up to a hole density of 2.0×10^{14} cm^{-2}, *i.e.*, added hole states carry equal magnetic moment. The maximum of ΔE_{mag} is reached at the

end of the plateau region and the value is much higher than for unstrained single-layer PbO, in agreement with the previous analysis of the DOS (enhancement of the electronic instability).

Fig. 5(c and d) addresses m and ΔE_{mag} for double- and triple-layer PbO, demonstrating the onset of ferromagnetism when the hole density reaches 0.2×10^{14} and 0.7×10^{14} cm^{-2}, respectively. However, the ferromagnetism vanishes again at hole densities of 1.6×10^{14} and 1.5×10^{14} cm^{-2}, respectively, *i.e.*, much earlier than for single-layer PbO. Double-layer PbO has a maximum of m = 0.88 μ_B per hole at a hole density of 0.9×10^{14} cm^{-2} and triple-layer PbO has a maximum of m = 0.61 μ_B per hole at a hole density of 1.0×10^{14} cm^{-2}. ΔE_{mag} behaves similar to m in both cases, reaching 0.74 meV at a hole density of 0.9×10^{14} cm^{-2} for double-layer PbO and 0.13 meV at a hole density of 1.0×10^{14} cm^{-2} for triple-layer PbO. The fact that we find no plateau in m, in contrast to single-layer PbO, indicates that quantum confinement plays an important role in the magnetic properties of hole-doped PbO. We also notice that single-layer PbO achieves much higher values of ΔE_{mag}, suggesting that it is more promising as a stable ferromagnetic platform than hole-doped multi-layer PbO.

If ferromagnetism occurs then the exchange energy gain exceeds the kinetic energy loss, or in the language of the Stoner Criterion[42,43] when $I \cdot \mathrm{DOS}(E_F) > 1$. Here E_F is the Fermi energy and I is the Stoner parameter that represents the strength of the exchange interaction.[44,45] Since $\mathrm{DOS}(E_F) \sim 0$ for single-layer PbO without hole doping, we have $I \cdot \mathrm{DOS}(E_F) < 1$ and thus a nonmagnetic state. When holes are introduced, the effective hole mass m_h determines $\mathrm{DOS}(E_F) \propto m_h^{3/2}(E_{VBM} - E_F)^{1/2}$. In the case of single-layer PbO the flat valence band edge results in large m_h. Therefore, $\mathrm{DOS}(E_F)$ increases with the hole density. In addition, the valence band edge of single-layer PbO is mainly due to O p orbitals, which host strong exchange interaction,[35] so that I is large for hole doping. Therefore, the product $I \cdot \mathrm{DOS}(E_F)$ becomes large enough to turn single-layer PbO into a ferromagnet.

We estimate the Curie temperature (T_c) based on the mean-field approximation *via* $k_B T_c = 2/3 \Delta E_{mag}$. The estimated T_c values for single-, double- and triple-layer PbO are 51 K, 6 K and 1 K, respectively. Because exchange splitting and the stability of the ferromagnetic state can be strongly enhanced by the biaxial tensile strain, the estimated T_c for strained single-layer PbO is 122 K, which is much higher than that of unstrained single- or multi-layer PbO.

In the present work, the electronic structures are calculated by using GGA, which always underestimates the band gap for insulators and semiconductors. We also calculate the band structure of single-layer PbO by using a hybrid functional approach and found that the band gap is 3.40 eV, which is 0.89 eV larger than the value from GGA. However, the band edge dispersion from the hybrid functional approach is very similar to that from GGA. Though Pb has large spin orbit interaction, the introduction of spin orbit interaction will reduce the calculated band gap a little bit, but has little effect on the magnetism of the PbO under hole doping and the easy axis of the magnetic moment keeps out of the plane.

Conclusion

In conclusion, we have employed first-principles calculations to investigate the influence of the sample thickness, applied strain, and hole doping on the electronic properties of PbO. For decreasing thickness both the VBM and CBM are found to shift to the Γ point, resulting in a direct band gap in the single-layer limit. We find for multi-layer PbO a Mexican-hat dispersion with indirect band gap, while single-layer PbO is characterized by a flat parabolic dispersion. Interestingly, the Mexican-hat dispersion reappears in single-layer PbO under biaxial tensile strain above 3%, inducing an indirect band gap. Both single- and multi-layer PbO develop half-metallicity under hole doping, where strain turns out to enhance the stability of the ferromagnetic state. *Via* mean-field approximation, we estimate a Curie temperature of T_c = 122 K for single-layer PbO under 6% biaxial tensile strain. We not only predict that ferromagnetism can be achieved in recently reported layered PbO, but also demonstrate that it originates from a van Hove singularity at the valence band edge. Our findings open a new avenue to realizing spintronics in single-layer oxides.

Acknowledgements

This work was financially supported by the National Natural Science Foundation of China (No. 11504169, 61575094 and 21673118), the National Basic Research Program of China (2015CB932200), the Natural Science Foundation of the Higher Education Institutions of Jiangsu Province, China (16KJB150018) and the Jiangsu Province Postgraduate Innovation Project. The research reported in this publication was supported by funding from King Abdullah University of Science and Technology (KAUST).

References

1 S. M. Yoon, H. J. Song and H. C. Choi, p-Type Semiconducting GeSe Combs by a Vaporization-Condensation-Recrystallization (VCR) Process, *Adv. Mater.*, 2010, **22**, 2164–2167.
2 A. M. Chockla, J. T. Harris and B. A. Korgel, Colloidal Synthesis of Germanium Nanorods, *Chem. Mater.*, 2011, **23**, 1964–1970.
3 D. Vaughn, D. Sun, S. M. Levin, A. J. Biacchi, T. S. Mayer and R. E. Schaak, Colloidal Synthesis and Electrical Properties of GeSe Nanobelts, *Chem. Mater.*, 2012, **24**, 3643–3649.
4 D. J. Xue, J. Tan, J. S. Hu, W. Hu, Y. G. Guo and L. J. Wan, Anisotropic Photoresponse Properties of Single Micrometer-Sized GeSe Nanosheet, *Adv. Mater.*, 2012, **24**, 4528–4533.
5 L. Li, Z. Chen, Y. Hu, X. Wang, T. Zhang, W. Chen and Q. Wang, Single-Layer Single-Crystalline SnSe Nanosheets, *J. Am. Chem. Soc.*, 2013, **135**, 1213–1216.
6 G. A. Tritsaris, B. D. Malone and E. Kaxiras, Optoelectronic Properties of Single-Layer, Double-Layer, and Bulk Tin Sulfide: A Theoretical Study, *J. Appl. Phys.*, 2013, **113**, 233507.

7 L. D. Zhao, S. H. Lo, Y. Zhang, H. Sun, G. Tan, C. Uher, C. Wolverton, V. P. Dravid and M. G. Kanatzidis, Ultralow Thermal Conductivity and High Thermoelectric Figure of Merit in SnSe Crystals, *Nature*, 2014, **508**, 373–377.

8 X.-H. Ma, K.-H. Cho and Y.-M. Sung, Growth Mechanism of Vertically Aligned SnSe Nanosheets *via* Physical Vapour Deposition, *CrystEngComm*, 2014, **16**, 5080–5086.

9 S. Larentis, B. Fallahazad and E. Tutuc, Field-Effect Transistors and Intrinsic Mobility in Ultra-Thin $MoSe_2$ Layers, *Appl. Phys. Lett.*, 2012, **101**, 223104.

10 H. Fang, S. Chuang, T. C. Chang, K. Takei, T. Takahashi and A. Javey, High Performance Single Layered WSe_2 p-FETs with Chemically Doped Contacts, *Nano Lett.*, 2012, **12**, 3788–3792.

11 P. Lu, X. Wu, W. Guo and X. C. Zeng, Strain-Dependent Electronic and Magnetic Properties of MoS_2 Monolayer, Bilayer, Nanoribbons and Nanotubes, *Phys. Chem. Chem. Phys.*, 2012, **14**, 13035–13040.

12 P. Tao, H. Guo, T. Yang and Z. Zhang, Strain-Induced Magnetism in MoS_2 Monolayer with Defects, *J. Appl. Phys.*, 2014, **115**, 054305.

13 D. Jariwala, V. K. Sangwan, L. J. Lauhon, T. J. Marks and M. C. Hersam, Emerging Device Applications for Semiconducting Two-Dimensional Transition Metal Dichalcogenides, *ACS Nano*, 2014, **8**, 1102–1120.

14 X. Xu, W. M. Yao, D. Xiao and T. F. Heinz, Spin and Pseudospins in Layered Transition Metal Dichalcogenides, *Nat. Phys.*, 2014, **10**, 343–350.

15 D. Ovchinnikov, A. Allain, Y. Huang, D. Dumcenco and A. Kis, Electrical Transport Properties of Single-Layer WS_2, *ACS Nano*, 2014, **8**, 8174–8181.

16 Y. Zhang, *et al.*, Direct Observation of the Transition from Indirect to Direct Bandgap in Atomically Thin Epitaxial $MoSe_2$, *Nat. Nanotechnol.*, 2014, **9**, 111–115.

17 L. Makinistian and E. A. Albanesi, First-Principles Calculations of the Band Gap and Optical Properties of Germanium Sulfide, *Phys. Rev. B: Condens. Matter Mater. Phys.*, 2006, **74**, 045206.

18 A. Rathor, V. Sharma, N. L. Heda, Y. Sharma and B. L. Ahuja, Compton Profiles and Band Structure Calculations of IV-VI Layered Compounds GeS and GeSe, *Radiat. Phys. Chem.*, 2008, **77**, 391–400.

19 G. Shi and E. Kioupakis, Anisotropic Spin Transport and Strong Visible-Light Absorbance in Few-Layer SnSe and GeSe, *Nano Lett.*, 2015, **15**, 6926–6931.

20 Y. Hu, S. Zhang, S. Sun, M. Xie, B. Cai and H. Zeng, GeSe Monolayer Semiconductor with Tunable Direct Band Gap and Small Carrier Effective Mass, *Appl. Phys. Lett.*, 2015, **107**, 122107.

21 S. Wolf, D. Awschalom, R. Buhrman, J. Daughton, S. Von Molnar, M. Roukes, A. Y. Chtchelkanova and D. Treger, Spintronics: A Spin-Based Electronics Vision for the Future, *Science*, 2001, **294**, 1488–1495.

22 S. J. Pearton, *et al.*, Wide Band Gap Ferromagnetic Semiconductors and Oxides, *J. Appl. Phys.*, 2003, **93**, 1–13.

23 K. Sato, *et al.*, First-Principles Theory of Dilute Magnetic Semiconductors, *Rev. Mod. Phys.*, 2010, **82**, 1633–1690.

24 A. Ramasubramaniam and D. Naveh, Mn-Doped Monolayer MoS_2: An Atomically Thin Dilute Magnetic Semiconductor, *Phys. Rev. B: Condens. Matter Mater. Phys.*, 2013, **87**, 195201.

25 L. Seixas, A. Carvalho and A. H. Castro Neto, Atomically Thin Dilute Magnetism in Co-Doped Phosphorene, *Phys. Rev. B: Condens. Matter Mater. Phys.*, 2015, **91**, 155138.

26 O. V. Yazyev and L. Helm, Defect-Induced Magnetism in Graphene, *Phys. Rev. B: Condens. Matter Mater. Phys.*, 2007, **75**, 125408.

27 O. V. Yazyev, Magnetism in Disordered Graphene and Irradiated Graphite, *Phys. Rev. Lett.*, 2008, **101**, 037203.

28 Y. Liu, F. Xu, Z. Zhang, E. S. Penev and B. I. Yakobson, Two-Dimensional Mono-Elemental Semiconductor with Electronically Inactive Defects: The Case of Phosphorus, *Nano Lett.*, 2014, **14**, 6782–6786.

29 H. Guo, N. Lu, L. Wang, X. Wu and X. C. Zeng, Tuning Electronic and Magnetic Properties of Early Transition-Metal Dichalcogenides *via* Tensile Strain, *J. Phys. Chem. C*, 2014, **118**, 7242–7249.

30 Y. Huang, C. Ling, H. Liu, S. Wang and B. Geng, Versatile Electronic and Magnetic Properties of $SnSe_2$ Nanostructures Induced by the Strain, *J. Phys. Chem. C*, 2014, **118**, 9251–9260.

31 T. Cao, Z. Li and S. G. Louie, Tunable Magnetism and Half-Metallicity in Hole-Doped Monolayer GaSe, *Phys. Rev. Lett.*, 2015, **114**, 236602.

32 S. Wu, X. Dai, H. Yu, H. Fan, J. Hu and W. Yao, Magnetisms in p-Type Monolayer Gallium Chalcogenides (GaSe, GaS), 2014, arXiv:1409.4733.

33 Y. Matsumoto, *et al.*, Room-Temperature Ferromagnetism in Transparent Transition Metal-Doped Titanium Dioxide, *Science*, 2001, **291**, 854–856.

34 J. M. D. Coey, M. Venkatesan and C. B. Fitzgerald, Donor Impurity Band Exchange in Dilute Ferromagnetic Oxides, *Nat. Mater.*, 2005, **4**, 173–179.

35 H. Peng, H. J. Xiang, S. H. Wei, S. S. Li, J. B. Xia and J. Li, Origin and Enhancement of Hole-Induced Ferromagnetism in First-Row d^0 Semiconductors, *Phys. Rev. Lett.*, 2009, **102**, 017201.

36 T. Dietl, A Ten-Year Perspective on Dilute Magnetic Semiconductors and Oxides, *Nat. Mater.*, 2010, **9**, 965–974.

37 A. K. Singh and R. G. Hennig, Computational Prediction of Two-Dimensional Group-IV Mono-Chalcogenides, *Appl. Phys. Lett.*, 2014, **105**, 042103.

38 T. Thonhauser, V. R. Cooper, S. Li, A. Puzder, P. Hyldgaard and D. C. Langreth, van der Waals density functional: Self-consistent potential and the nature of the van der Waals bond, *Phys. Rev. B: Condens. Matter Mater. Phys.*, 2007, **76**, 125112.

39 T. Thonhauser, S. Zuluaga, C. A. Arter, K. Berland, E. Schroder and P. Hyldgaard, Spin Signature of Nonlocal Correlation Binding in Metal-Organic Frameworks, *Phys. Rev. Lett.*, 2015, **115**, 136402.

40 P. Giannozzi, *et al.*, QuantumESPRESSO: A Modular and Open-Source Software Project for Quantum Simulations of Materials, *J. Phys.: Condens. Matter*, 2009, **21**, 395502.
41 D. Wickramaratne, F. Zahid and R. K. Lake, Mexican Hat and Rashba Bands in Few-Layer van der Waals Materials, 2014, arXiv:1412.2090.
42 E. C. Stoner, Collective Electron Ferromagnetism, *Proc. R. Soc. A*, 1938, 372–414.
43 E. C. Stoner, Collective Electron Ferromagnetism. II. Energy and Specific Heat, *Proc. R. Soc. A*, 1939, 339–371.
44 L. Fritsche and B. Weimert, First-Principles Theory of Ferromagnetic and Antiferromagnetic Order, *Phys. Status Solidi B*, 1998, **208**, 287–338.
45 L. Fritsche and J. Koller, Potentials in Density Functional Theory and the Importance of Sum Rules, *J. Solid State Chem.*, 2003, **176**, 652–670.

